Materials Science in Semiconductor Processing 200 (2025) 110003

Contents lists available at ScienceDirect

Materials Science in Semiconductor Processing

journal homepage: www.elsevier.com/locate/mssp

Effect of oxygen content on *p*-type electrical conductivity in β-Ga_2O_3 films

Se-Rim Park [a,b], Zeyu Chi [b,*], Corinne Sartel [b], Sang-Mo Koo [a], Mathieu Fregnaux [c], Yunlin Zheng [d], Sean Douglas [e], Lewis Penman [e], Fabien Massabuau [e], Tamar Tchelidze [f], Jean-Michel Chauveau [b,**], Ekaterine Chikoidze [b,***]

[a] Department of Electronic Materials Engineering, Kwangwoon University, Seoul, 01897, Republic of Korea
[b] Groupe d'Etude de la Matière Condensée (GEMaC), Université Paris-Saclay, UVSQ, CNRS, 45 Av. des Etats-Unis, Versailles Cedex, 78035, France
[c] Institut Lavoisier de Versailles (ILV), Université Paris-Saclay, UVSQ – CNRS, 45 Av. des Etats-Unis, Versailles, Cedex, 78035, France
[d] Institut des Nano Sciences de Paris (INSP), CNRS UMR7588, Sorbonne Université, 4 place Jussieu, 75252, Paris, France
[e] Department of Physics, SUPA, University of Strathclyde, 107 Rottenrow East, Glasgow, G4 0NG, UK
[f] Faculty of Exact and Natural Science, Department of Physics, Ivane Javakhishvili Tbilisi State University, 3 Av. Tchavtchavadze, 0179, Tbilisi, Georgia

ARTICLE INFO

Keywords:
β-Ga_2O_3
p-type conductivity
Homoepitaxy
Oxygen content

ABSTRACT

β-Ga_2O_3 is a promising ultrawide bandgap semiconductor, but achieving reliable *p*-type conductivity remains a challenge, especially due to the scarcity of high-quality homoepitaxial *p*-type β-Ga_2O_3 layers. In this study, we investigate β-Ga_2O_3 thin films homoepitaxially grown on $(\bar{2}01)$ Fe doped β-Ga_2O_3 substrates via metal organic chemical vapor deposition under different oxygen-to-gallium (O/Ga) ratios. We examine the effect of oxygen content on the structural, electrical, and optical properties of thin films. The layer grown under oxygen-rich conditions (O/Ga = 6400) exhibited an enhanced crystallinity of the dominant $(\bar{2}01)$ orientation as indicated by a low full-width at half maximum (FWHM) of 72 arcsec in the X-ray diffraction rocking curve, a suppressed oxygen vacancy signal in X-ray photoelectron spectroscopy, and a two order of magnitude increase in hole concentration ($p = 4.5 \times 10^{15}$ cm^{-3} *vs.* 4.6×10^{13} cm^{-3} at 570 K), associated with a shallow acceptor level with an activation energy of 0.21 eV, likely due to V_{Ga}^{-}- V_O^{++} complex-like defect. In addition, both films exhibit hole mobility $\mu_H > 30$ $cm^2/V{\cdot}s$ over the measurement temperature range. These findings suggest that oxygen-rich growth conditions enhance both the crystallinity and native hole conductivity of β-Ga_2O_3, offering a promising route toward achieving controlled *p*-type behavior in this material.

1. Introduction

Gallium oxide (Ga_2O_3) has garnered significant attention due to its exceptional properties, such as an ultrawide bandgap of 4.6–4.9 eV and a high breakdown electric field larger than 8 MV/cm [1,2]. These outstanding characteristics make Ga_2O_3 promising material for various applications, including UV optoelectronics [3] and power electronic devices [4–8]. Ga_2O_3 crystallizes in several polymorphic forms, including α, β, γ, δ, and κ, with the monoclinic β-Ga_2O_3 phase identified as the thermodynamically stable structure [9].

To date, Ga_2O_3-based devices have primarily been developed as unipolar devices relying on *n*-type doping. However, realizing the requirements of Ga_2O_3 for more advanced applications requires bipolar doping, necessitating the capability for both *n*-type and *p*-type doping. Realizing *p*-type doping in ultrawide bandgap semiconductors oxides, particularly Ga_2O_3, remains a challenge due to the large acceptor ionization energy by theoretical prediction [10]. Efforts to achieve effective *p*-type conductivity have focused on doping with elements such as Zn [1,11–13], Mg [14], N [15], H [16] and P [17–19], as well as co-doping strategies [20,21].

Metal organic chemical vapor deposition (MOCVD) is widely regarded as one of the most effective techniques for growing high-quality β-Ga_2O_3 thin films [22–24]. Growth conditions in MOCVD significantly affect the conductivity and properties of β-Ga_2O_3 thin films by influencing the formation and interaction of intrinsic defects [25,26]. The choice of substrate – native (homoepitaxy) or foreign

* Corresponding author.
** Corresponding author.
*** Corresponding author.
E-mail addresses: zeyu.chi@uvsq.fr (Z. Chi), jean-michel.chauveau@uvsq.fr (J.-M. Chauveau), ekaterine.chikoidze@uvsq.fr (E. Chikoidze).

https://doi.org/10.1016/j.mssp.2025.110003
Received 25 June 2025; Received in revised form 9 August 2025; Accepted 24 August 2025

(heteroepitaxy) – also significantly influences the crystalline quality of the layers. While significant advancements have been made in the growth of high quality *n*-type homoepitaxial β-Ga_2O_3 thin-films on different crystallographic orientations by several growth methods including MOCVD [27–30], there are relatively few demonstration of homo *p-n* junction [31]. To address efficiently the need of *p-n* homojunction realization, the first necessary condition is to grow *p*-type β-Ga_2O_3 layers.

In this work, we study two homoepitaxial β-Ga_2O_3 thin films grown on $(\bar{2}01)$-oriented β-Ga_2O_3 substrates grown by MOCVD. We systematically investigate the influence of oxygen content on the crystalline structure, electrical, and optical properties of two β-Ga_2O_3 films. Our results show that oxygen-rich growth enhances crystalline quality, reduces oxygen vacancy concentration, and enables improved hole conductivity at elevated temperatures with remarkably high hole mobilities. These findings contribute to a better understanding of the impact of oxygen stoichiometry on hole transport in β-Ga_2O_3 and support further exploration of controlled *p*-type doping strategies in homoepitaxial films.

2. Results and discussion

Two undoped β-Ga_2O_3 epilayers were grown by MOCVD on Fe-doped $(\bar{2}01)$ β-Ga_2O_3 substrates at 825 °C. The flows of TMGa and O_2 were set at 36 μmol/min and 1500 sccm, and 12 μmol/min and 1200 sccm, respectively. The ratios of O/Ga were determined to be 2700 and 6400, respectively, therefore we will refer to the samples as O/Ga (2700) and O/Ga (6400). The growth details can be found in experimental methods section.

2.1. Structural and compositional analysis

Fig. 1(a) shows the XRD $\theta/2\theta$ scans for samples O/Ga (2700) and O/Ga (6400). Both samples exhibit $(\bar{2}01)$ preferred growth orientation, with the $\bar{2}01$, $\bar{4}02$, $\bar{6}03$ and $\bar{8}04$ reflections. However, additional tiny peaks other than $\{\bar{2}01\}$ family are observed in the $\theta/2\theta$ scan of sample O/Ga (6400), especially in sample O/Ga (6400), with intensities nearly five orders of magnitude lower than the main reflections. The corresponding rocking curves show a mixture of sharp or broad peaks with varying orientations to the normal ($\Delta\omega = 0$), further indicating that these tiny peaks are not attributed to polycrystalline rings, but linked to particular crystallites oriented in a defined way. This observation may be attributed to excessive oxygen supply during growth, which enhances the pre-reactions, leading to the formation of randomly oriented grains [25]. Similar observations have also been reported in MOCVD and other growth systems [23,25,32]. The structural quality of the films was further investigated by ω-scans (Fig. 1(b)). Sample O/Ga (2700) shows full width at half maximum (FWHM) of 0.04° (~144 arcsec), while Sample O/Ga (6400) exhibits a lower FWHM of 0.02° (~72 arcsec), suggesting that the increased oxygen content promotes higher crystallinity. These tiny FWHM values indicate the great crystallinity of the homoepitaxially grown layers, smaller than that of the substrate (1080 arcsec) before the growth.

Fig. 1(c) shows the Raman spectroscopy results recorded in the range of 130–800 cm^{-1} using 514.5 nm excitation for (−201) β-Ga_2O_3 single crystal and homoepitaxial layers. Both samples exhibit the well-known Raman active phonon modes of β-Ga_2O_3 without any signature belonging to other Ga_2O_3 polymorphs, confirming the absence of secondary phase. [33,34]. These modes can be grouped into three parts: (a) low frequency modes (100–200 cm^{-1}) originate from liberations and translations of the Ga_IO_4 tetrahedral and $Ga_{II}O_6$ octahedral chains; (b) mid frequency modes (~310–480 cm^{-1}) correspond to deformation of $Ga_{II}O_6$ octahedra; (c) high frequency modes (~500–770 cm^{-1}) arise from stretching and bending of Ga_IO_4 tetrahedral chains [35,36]. Notably, a pronounced difference in peak intensities of high frequency modes (A_g (7) – A_g (10) and B_g (5)) is observed between samples, without significant peak shift across the whole range. This suggests that the variation in oxygen content during MOCVD growth led to local lattice perturbations instead of polyhedral framework, particularly affecting the Ga_IO_4 tetrahedral chains.

Chemical composition analysis of the β-Ga_2O_3 thin films was obtained by XPS, with data shown in Fig. 2. It should be noted that such quantitative surface analyses require important considerations to obtain reliable, and useful information. When conducted on rough or non-conductive samples, shadowing and charging effects can distort XPS signals [37]. In our case, considering the sample's conductivity, flood gun was used for charge compensation.

The Ga3*d* spectral region was deconvoluted into three components (Fig. 2(a)). Two main peaks at 19.0 and 20.0 eV were assigned to Ga^+

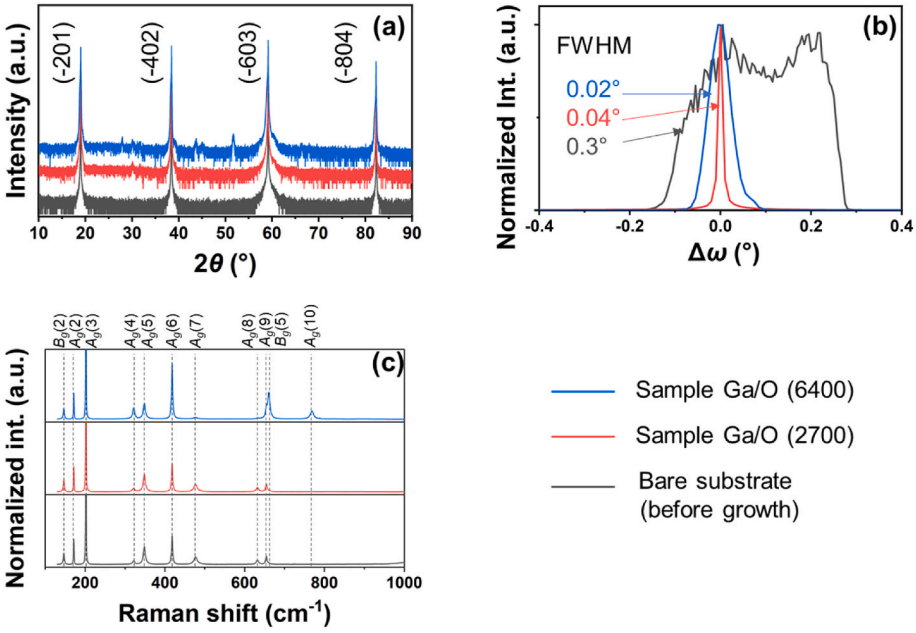

Fig. 1. (a) XRD out of plane $\theta/2\theta$ scans, (b) ω-scan rocking curves of $\bar{4}02$ reflection (c) Raman spectra of β-Ga_2O_3 thin films with bare substrate before epitaxy.

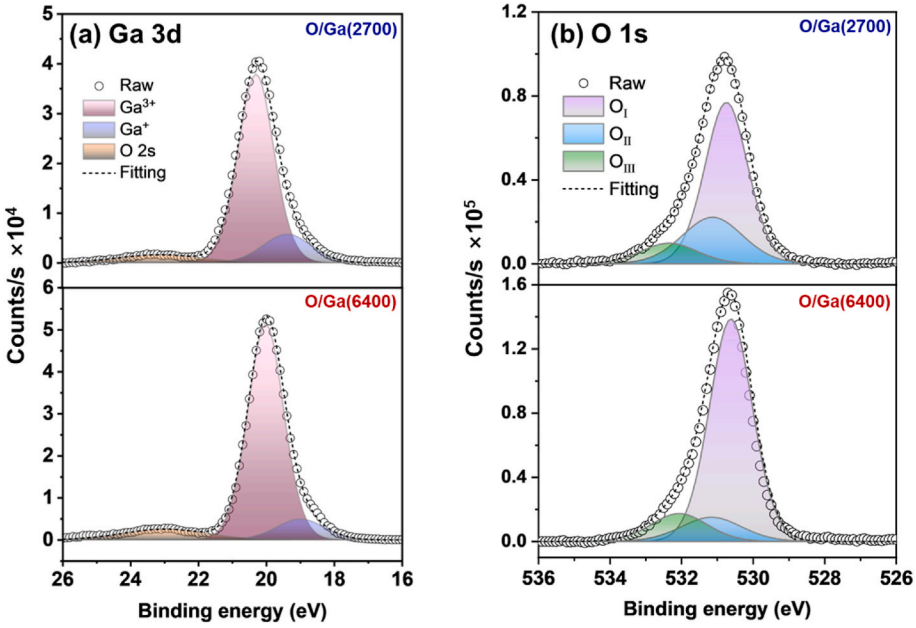

Fig. 2. XPS spectra core level of β-Ga_2O_3 thin films: (a) Ga3*d* and (b) O1*s* spectral regions.

and Ga^{3+} states, respectively [38]. A weak additional peak at 23.0 eV was attributed to the overlapping O2*s* peak [39]. As the O/Ga ratio during growth increased from 2700 to 6400, the area ratio of $Ga^{+}/(Ga^{+}+Ga^{3+})$ decreased from 17 % to 11 %. The Ga^{+} indicates a lattice oxygen deficiency and thus indicates the presence of oxygen vacancies (V_O) [40,41]. The reduction in the Ga^{+} component in sample O/Ga (6400) suggests that additional oxygen was incorporated, owing to the higher O/Ga ratio, thereby reducing V_O density and promoting conversion of Ga^{+} to Ga^{3+}.

The O1*s* spectra were fitted with three components: The O_I peak at 530.0–531.0 eV [42], attributed to Ga–O bonding, the O_{II} peak at 531.0–532.0 eV [43] related to the surface species: oxygen vacancies (V_O), and the O_{III} peak at 532.0–533.0 eV [44] related to hydroxyl (-OH) or carbonate species in films, as well as physisorbed species (Fig. 2(b)). To compare the relative V_O concentrations in β-Ga_2O_3 thin films, the area ratio of $O_{II}/(O_I + O_{II})$ was calculated. Sample O/Ga (2700) showed an $O_{II}/(O_I + O_{II})$ ratio of 28 %, while the sample O/Ga (6400) sample exhibited a reduced ratio of 13 %, suggesting a lower V_O density near the surface of sample O/Ga (6400). These results are consistent with the trends observed in the Ga3*d* spectra (Fig. 2(a)).

2.2. Electrical transport properties

The effect of different O/Ga ratios on the electrical properties of the

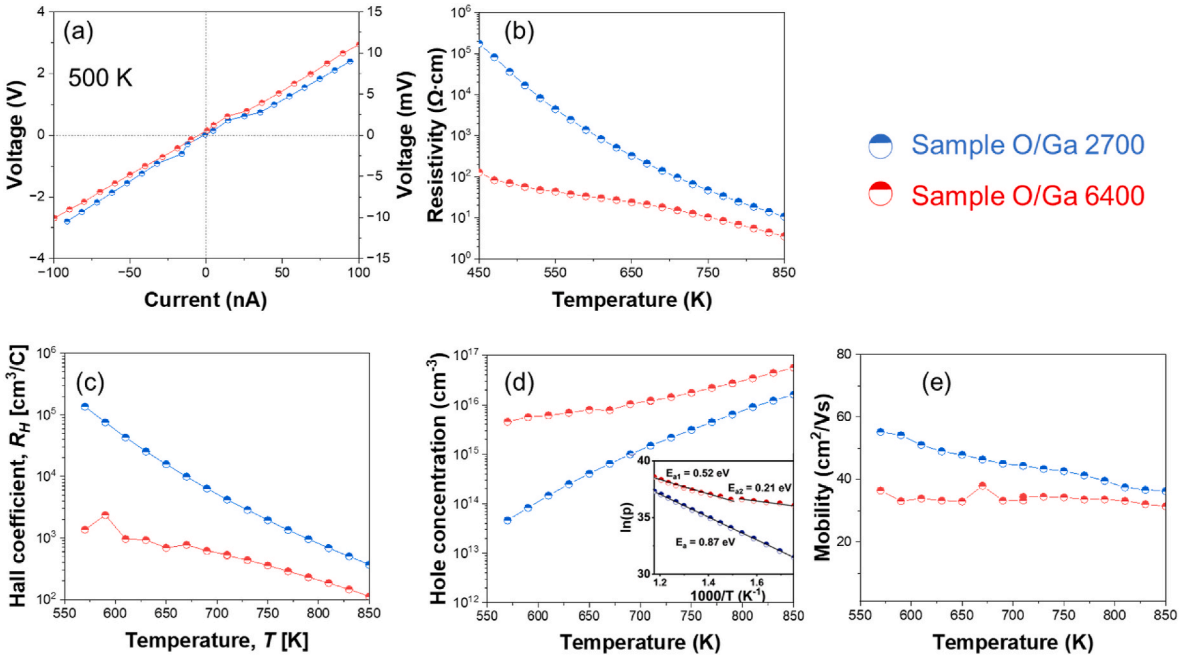

Fig. 3. (a) *I-V* characteristics at 500 K. (b) Temperature dependent resistivity in the range of 450–850 K. (c) Hall coefficients *vs.* temperature (d) Temperature-dependent Hall hole concentrations. The inset shows the Arrhenius plot (ln(*p*) versus 1000/*T*) used to determine the carrier activation energies. (e) Hall hole mobilities versus temperature.

samples was investigated. Ohmic contacts were formed by silver paste at the four corners of the square-shaped sample in a Van der Pauw configuration. Linear *I-V* characteristics at 500 K indicated the Ohmic behavior (Fig. 3 (a)). In the temperature range of 450–850 K, the resistivities decreased from $\rho = 1.8 \times 10^5$ Ω•cm to 10.7 Ω cm in sample O/Ga (2700), and from $\rho = 1.3 \times 10^2$ Ω•cm to 3.5 Ω cm in sample O/Ga (6400) (Fig. 3 (b)).

Measurement down to room temperature was limited due to the high resistivity at such temperatures. Electrical transport measurements showed that the higher oxygen contents in the O/Ga (6400) sample leads to improved electrical conductivity. The *p*-type conduction is evidenced by consistently positive Hall coefficients over measurement temperature range between 570 and 850 K as shown in Fig. 3 (c). The temperature dependence of the Hall hole concentration is shown in Fig. 3 (d). The Hall hole concentration at $T = 570$ K for sample O/Ga (2700) and sample O/Ga (6400) was $p = 4.6 \times 10^{13}$ cm^{-3} and $p = 4.5 \times 10^{15}$ cm^{-3}, respectively. This trend agrees with previous reports showing that oxygen annealing reduces V_O-related compensation and enhances hole concentration in undoped β-Ga_2O_3 thin films [45]. The mobility was determined to be in the range of 35–55 cm^2/V·s for O/Ga (2700) and 31–36 cm^2/V·s for O/Ga (6400) across the entire temperature range (Fig. 3 (e)).

The carrier activation energies were determined from a linear region of Arrhenius plot (ln(*p*) versus 1000/*T*) shown in the inset of Fig. 3 (d). A single slope with an activation energy of $E_a = 0.87 \pm 0.01$ eV was found for sample O/Ga (2700), probably related with gallium vacancy (V_{Ga}). Two slopes with two different activation energies, $E_{a1} = 0.52 \pm 0.02$ eV at high temperature and $E_{a2} = 0.21 \pm 0.02$ eV at low temperature, were distinguished for sample O/Ga (6400). E_{a1} lies close to the reported V_{Ga}-related deep acceptor center activation energy in the low compensation regime, and E_{a2} might be related with another shallower acceptor V_{Ga}^{-}-V_O^{++} complexes defect's electrical activation as was already reported [45]. The creation of this defect is favorable in oxygen rich conditions (less V_O) promoting the recharging of V_O^{+} into V_O^{++} leading the pairing with V_{Ga}^{-} defect [46]. Evidently, the probability of defects pairing strongly depends on the concentration of native defects (V_O; V_{Ga}) and the vicinity of their positions. These favorable conditions can be determined by the growth parameters (temperature, pressure) and the crystal structure. Similar temperature dependent resistivity have been previously reported for β-Ga_2O_3/Al_2O_3 thin films [45,47,48]. But it is worth noting that the homoepitaxial layers exhibit hole mobility of around 3 times higher compared to the β-Ga_2O_3/Al_2O_3 layer ($\mu \sim 10$ cm^2/(V·s) at 850 K) [45], which can be attributed to its significantly improved structural properties. This provides additional evidence that holes can move more freely in β-Ga_2O_3. These enhanced mobilities are reproducible and repeatable, a detailed study on the electrical properties of additional samples will be presented in a separate article currently under review.

2.3. Optical properties

Fig. 4(a)–(b) show the temperature-dependent PL spectra for both samples, with the decomposition of the 25 K spectrum shown in Fig. 4 (c)–(d). The PL spectra of both samples conform to existing literature, exhibiting broad luminescence spanning *ca.* 2–4 eV and a Gaussian decomposition into *ca.* 3.5 eV, 3.0–3.1 eV, and 2.4 eV lines [49–53]. The 3.5 eV peak refers to the recombination between free electrons and localized holes at low temperatures [54]. The 3.0–3.1 eV peak corresponds to donor-acceptor pair (DAP) transitions involving V_O and V_{Ga} [51,55], while the 2.4 eV line is associated with DAP transitions involving O_i [51,52,56].

As shown in Fig. 4(a)–(b), the PL intensity of both samples decreases as the temperature increased from 25 to 300 K. Notably, sample O/Ga (2700) exhibits significantly stronger thermal quenching compared to sample O/Ga (6400). The integrated PL intensity of sample O/Ga (2700) decays by a factor of 130, while that of sample O/Ga (6400) decays by only a factor of 15.

Additionally, a difference in peak wavelength shift with temperature was observed between the samples. Sample O/Ga (6400) exhibits a gradual redshift of *ca.* 320 meV as temperature increases, whereas sample O/Ga (2700) initially shows a slight redshift of *ca.* 40 meV at low temperatures, followed by a blueshift of *ca.* 30 meV as the temperature rises further. For sample O/Ga (6400), the redshift seems to come from a more pronounced decrease in the 3.5 eV line, with negligible change (and even, slight increase) in DAP transitions (2.4 eV and 3.1 eV lines). This behavior is consistent with electrical measurements, where holes can be more easily delocalized in that sample. The redshift commonly observed in samples with multiple luminescence centers, can be attributed to the migration or relaxation of localized carriers from shallower to deeper centers. In contrast, for sample O/Ga (2700), a more uniform

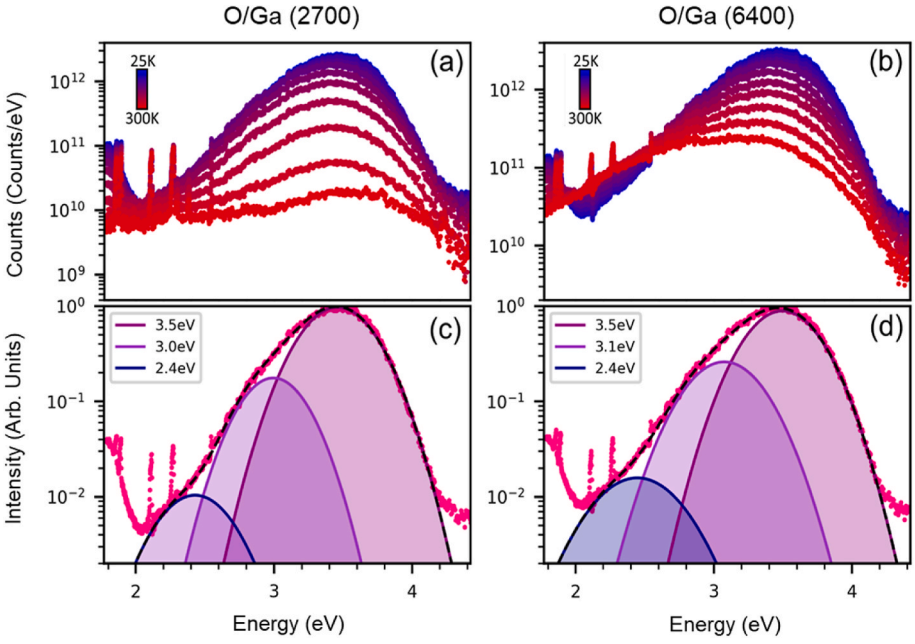

Fig. 4. (a) (b) Temperature-dependent PL from 25 to 300 K. (c) (d) Deconvolution of 25 K PL spectra.

decrease in intensity across all luminescence lines is observed, which could suggest that thermally excited carriers are not re-trapped to recombine radiatively but instead recombine non-radiatively, which is consistent with the greater thermal quenching and lower crystalline quality we observed by XRD on this sample.

3. Conclusion

In summary, β-Ga_2O_3 thin films were grown on Fe-doped $(\bar{2}01)$ β-Ga_2O_3 substrates by MOCVD under two different O/Ga ratios of 2700 and 6400. A systematic investigation reveals that, while minor off-oriented domains are observed in oxygen-rich sample, higher oxygen supply (O/Ga = 6400) enhances crystalline coherence and reduces mosaicity, decreases surface oxygen vacancies, and significantly improves hole conductivity. This is supported by a narrower FWHM in XRD and a suppressed V_O signal in XPS, confirming the structural and chemical improvement. Raman analysis confirms the absence of other Ga_2O_3 polymorphs in both samples. Temperature-dependent Hall effect measurements show enhanced electrical transport properties in sample O/Ga (6400), with a hole concentration of $p = 4.5 \times 10^{15}$ cm^{-3} 570 K, (while $p = 4.6 \times 10^{13}$ cm^{-3} in sample O/Ga (2700)). Additionally, the presence of two distinct activation energies suggests contributions from both deep (0.52 eV) and shallow (0.21 eV) acceptor states, with the latter one likely related to the $V_{Ga}^{-} - V_O^{++}$ complex defects, which are more favored under oxygen-rich conditions. PL spectra show three emission peaks at (3.5 eV, 3.0–3.1 eV, and 2.4 eV) in both samples. Notably, the O/Ga (2700) sample exhibited pronounced thermal quenching, indicating a greater non-radiative recombination rate. In addition, both thin films exhibit hole mobilities of $\mu > 30$ cm^2/(V·s) across the measurement temperature range, supporting the presence of mobile hole transport at elevated temperatures. These findings highlight the influence of oxygen stoichiometry on the structural quality and high-temperature transport behavior of β-Ga_2O_3.

CRediT authorship contribution statement

Se-Rim Park: Writing – review & editing, Writing – original draft, Visualization, Methodology, Investigation, Funding acquisition, Formal analysis, Data curation. **Zeyu Chi:** Writing – review & editing, Visualization, Validation, Supervision, Project administration, Methodology, Investigation, Formal analysis, Data curation, Conceptualization. **Corinne Sartel:** Resources, Investigation. **Sang-Mo Koo:** Supervision, Funding acquisition. **Mathieu Fregnaux:** Methodology, Investigation, Formal analysis. **Yunlin Zheng:** Methodology, Investigation, Formal analysis. **Sean Douglas:** Visualization, Methodology, Investigation, Formal analysis, Conceptualization. **Lewis Penman:** Visualization, Resources, Methodology, Investigation. **Fabien Massabuau:** Writing – review & editing, Visualization, Validation, Supervision, Resources, Methodology, Investigation, Funding acquisition, Formal analysis. **Tamar Tchelidze:** Writing – review & editing, Validation, Software, Formal analysis. **Jean-Michel Chauveau:** Writing – review & editing, Supervision, Funding acquisition, Formal analysis. **Ekaterine Chikoidze:** Writing – review & editing, Validation, Supervision, Resources, Methodology, Funding acquisition, Formal analysis, Conceptualization.

Experimental methods

Thin film growth: Two undoped β-Ga_2O_3 epilayers 1 μm thick were grown by MOCVD on Fe-doped $(\bar{2}01)$ β-Ga_2O_3 substrates purchased from Novel Crystal Technology. For both samples, the growth temperature was set at 825 °C, the total pressure was maintained at 33 Torr. Trimethylgallium (TMGa) and high-purity oxygen (O_2) were used as precursors for Ga and O, respectively. The flows of TMGa and O_2 were set at 36 μmol/min and 1500 sccm, and 12 μmol/min and 1200 sccm, respectively. The ratios of O/Ga for two samples were determined to be 2700 and 6400, respectively.

X-ray diffraction (XRD): The crystalline structure of the films was characterized using XRD. $\theta/2\theta$ scans and rocking-curves (ω-scans) were performed to evaluate the crystalline quality and orientational spread of the films. Data were collected on a 5-circle diffractometer (Rigaku SmartLab) with Cu $K_{\alpha 1}$ radiation from a rotating anode and selected by a channel-cut Ge (220) × 2 monochromator.

Raman: Raman spectra were recorded using a Renishaw Invia Reflex micro-Raman spectrometer at room temperature. The samples were excited using a cw Modu-Laser Stellar-REN laser emitting at 514.5 nm with a power of 2–4 mW. Thereflecting microscope objective was 50 × with a NA 0.75; the excitation spot diameter was 1 μm. The back-scattered light was dispersed by a mono chromator with a spectral resolution of 1.4 cm^{-1}. The light was detected by a charge coupled device. The typical accumulation time was 30 s.

Electrical measurements: A custom-built set-up for high-impedance measurements was used for the investigation of the electrical transport measurements. Ohmic contacts were prepared using silver paint at the four corners of the sample. Hall effect measurements were performed in a Van der Pauw configuration, over the temperature range of 300–850 K, with magnetic fields perpendicularly applied to the film plane at 1.6 T. Temperature dependent measurements were carried out under a magnetic field of 1.6 T.

X-ray photoemission spectroscopy (XPS): XPS measurements were conducted on a Thermo Fisher Scientific Escalab 250 xi equipped with a monochromated Al-Kα anode (1486.6 eV) and a dual flood gun (low energy electron and ion). High energy resolution spectral windows of interest were recorded with a 650 μm spot. Photoelectron detection was performed perpendicular to the surface in constant analyzer energy (CAE) mode (10 eV pass energy) and in 0.1 eV energy step. β-Ga_2O_3 films and the substrate underneath being resistive, the use of low-energy electron and ion flood gun was required to perform the analysis. Quantification was done using the Thermo Fisher Scientific Avantage© software. Chemical compositions were obtained from the C 1s, O 1s, Ga 3d peak areas after a Shirley type background subtraction and considering "AlThermo1" sensitivity factor library.

Photoluminescence (PL) spectra: The luminescence properties of the samples were acquired on a custom-built PL setup driven by a Photon Systems 224 nm HeAg laser pulsed at a frequency of 20 Hz. The samples were mounted on a cold stage which incorporates a liquid He based closed-loop cryostat. The emitted light from the sample is directed to a spectrometer which is composed of a 400 l/mm ruled diffraction grating blazed at 325 nm, and an Andor CCD camera. A 280 nm long-pass filter is utilized at the opening aperture of the spectrometer to filter out any laser light. During the experiment the samples were cooled to a temperature of 25 K, then the temperature was raised by 25 K steps until 300 K. The resulting PL spectra were corrected for system response. The deconvolution of the low temperature spectra was performed manually by using the FitYK software package.

Declaration of competing interest

The authors declare that they have no known competing financial interests or personal relationships that could have appeared to influence the work reported in this paper.

Acknowledgements

The work in France has been funded by French National Agency of Research (ANR), project "GOPOWER", CE-50 N0015-01 and MRSEI PHC-Maimonide N50047TD.

Dr. E. Chikoidze would acknowledge IRP-CNRS "GALLIA" project giving possibility to cooperate with colleagues from University of Strathclyde.

The work has been funded by the Engineering and Physical Sciences Research Council (grants EP/W524670/1, EP/V034995/1) and UK

Space Agency's Enabling Technologies Programme UK Space Agency (UKSAG23_0043_ETP4-052).

Serim Park acknowledges Fostering Global Talents for Innovative Growth Program through KIAT of the MOTIE (P0017308), the France 2030 programme "ANR-11-IDEX-0003″ via Integrative Institute of Materials from Paris-Saclay University - 2IM@UPSaclay.

Data availability

Data will be made available on request.

References

[1] E. Chikoidze, T. Tchelidze, C. Sartel, Z. Chi, R. Kabouche, I. Madaci, C. Rubio, H. Mohamed, V. Sallet, F. Medjdoub, A. Perez-Tomas, Y. Dumont, Ultra-high critical electric field of 13.2 MV/cm for Zn-doped p-type β-Ga2O3, Mater. Today Phys. 15 (2020) 100263, https://doi.org/10.1016/j.mtphys.2020.100263.

[2] M. Higashiwaki, K. Sasaki, A. Kuramata, T. Masui, S. Yamakoshi, Gallium oxide (Ga2O3) metal-semiconductor field-effect transistors on single-crystal β-Ga2O3 (010) substrates, Appl. Phys. Lett. 100 (2012) 013504, https://doi.org/10.1063/1.3674287.

[3] H. Chen, Z. Li, Z. Zhang, D. Liu, L. Zeng, Y. Yan, D. Chen, Q. Feng, J. Zhang, Y. Hao, C. Zhang, Review of β-Ga2O3 solar-blind ultraviolet photodetector: growth, device, and application, Semicond. Sci. Technol. 39 (2024) 063001, https://doi.org/10.1088/1361-6641/ad42cb.

[4] W. Li, D. Saraswat, Y. Long, K. Nomoto, D. Jena, H.G. Xing, Near-ideal reverse leakage current and practical maximum electric field in β-Ga2O3 Schottky barrier diodes, Appl. Phys. Lett. 116 (2020) 192101, https://doi.org/10.1063/5.0007715.

[5] C.-H. Lu, F.-G. Tarntair, Y.-C. Kao, N. Tumilty, R.-H. Horng, Undoped β-Ga2O3 layer thickness effect on the performance of MOSFETs grown on a sapphire substrate, ACS Appl. Electron. Mater. 6 (2024) 568–575, https://doi.org/10.1021/acsaelm.3c01558.

[6] T.D. Nguyen, Q. Tu, X. Zhang, Y.C. Lin, A printed gallium oxide dielectric for 2D transistors, Nat. Electron. 7 (2024) 1078–1079, https://doi.org/10.1038/s41928-024-01307-9.

[7] J. Zhang, P. Dong, K. Dang, Y. Zhang, Q. Yan, H. Xiang, J. Su, Z. Liu, M. Si, J. Gao, M. Kong, H. Zhou, Y. Hao, Ultra-wide bandgap semiconductor Ga2O3 power diodes, Nat. Commun. 13 (2022) 3900, https://doi.org/10.1038/s41467-022-31664-y.

[8] F. Zhou, H. Gong, M. Xiao, Y. Ma, Z. Wang, X. Yu, L. Li, L. Fu, H.H. Tan, Y. Yang, F.-F. Ren, S. Gu, Y. Zheng, H. Lu, R. Zhang, Y. Zhang, J. Ye, An avalanche-and-surge robust ultrawide-bandgap heterojunction for power electronics, Nat. Commun. 14 (2023) 4459, https://doi.org/10.1038/s41467-023-40194-0.

[9] Z. Chi, J.J. Asher, M.R. Jennings, E. Chikoidze, A. Pérez-Tomás, Ga_2O_3 and related ultra-wide bandgap power semiconductor oxides: new energy electronics solutions for CO_2 emission mitigation, Materials 15 (2022) 1164, https://doi.org/10.3390/ma15031164.

[10] A. Kyrtsos, M. Matsubara, E. Bellotti, On the feasibility of p-type Ga_2O_3, Appl. Phys. Lett. 112 (2018) 032108, https://doi.org/10.1063/1.5009423.

[11] Z. Chi, C. Sartel, Y. Zheng, S. Modak, L. Chernyak, C.M. Schaefer, J. Padilla, J. Santiso, A. Ruzin, A.-M. Gonçalves, J. von Bardeleben, G. Guillot, Y. Dumont, A. Pérez-Tomás, E. Chikoidze, Native defects association enabled room-temperature p-type conductivity in β-Ga2O3, J. Alloys Compd. 969 (2023) 172454, https://doi.org/10.1016/j.jallcom.2023.172454.

[12] E. Chikoidze, C. Sartel, H. Yamano, Z. Chi, G. Bouchez, F. Jomard, V. Sallet, G. Guillot, K. Boukheddaden, A. Pérez-Tomás, T. Tchelidze, Y. Dumont, Electrical properties of p-type Zn:Ga2O3 thin films, J. Vac. Sci. Technol. A 40 (2022) 043401, https://doi.org/10.1116/6.0001766.

[13] T.D. Gustafson, J. Jesenovec, C.A. Lenyk, N.C. Giles, J.S. McCloy, M.D. McCluskey, L.E. Halliburton, Zn acceptors in β-Ga2O3 crystals, J. Appl. Phys. 129 (2021) 155701, https://doi.org/10.1063/5.0047947.

[14] M.H. Wong, C.-H. Lin, A. Kuramata, S. Yamakoshi, H. Murakami, Y. Kumagai, M. Higashiwaki, Acceptor doping of β-Ga2O3 by Mg and N ion implantations, Appl. Phys. Lett. 113 (2018) 102103, https://doi.org/10.1063/1.5050040.

[15] Y. Lu, L. Jia, D. Chen, T. Li, H. Qi, X. Xu, X. Li, M. Zhu, H. Zhang, X. Lu, Insight into the high hole concentration of p-Type Ga2O3 via in situ nitrogen doping, J. Phys. Chem. Lett. 16 (2025) 4243–4251, https://doi.org/10.1021/acs.jpclett.5c00318.

[16] M.M. Islam, M.O. Liedke, D. Winarski, M. Butterling, A. Wagner, P. Hosemann, Y. Wang, B. Uberuaga, F.A. Selim, Chemical manipulation of hydrogen induced high p-type and n-type conductivity in Ga_2O_3, Sci. Rep. 10 (2020) 6134, https://doi.org/10.1038/s41598-020-62948-2.

[17] Z. Chi, S.-R. Park, L. Burdiladze, T. Tchelidze, J.-M. Chauveau, Y. Dumont, S.-M. Koo, Z. Kushitashvili, A. Bibilashvili, G. Guillot, A. Pérez-Tomás, X.-Y. Tsai, F.-G. Tarntair, R.H. Horng, E. Chikoidze, Anderson disorder related *p*-type conductivity and metal-insulator transition in *β*-Ga2O3, Mater. Today Phys. 49 (2024) 101602, https://doi.org/10.1016/j.mtphys.2024.101602.

[18] R.H. Horng, X.-Y. Tsai, F.-G. Tarntair, J.-M. Shieh, S.-H. Hsu, J.P. Singh, G.-C. Su, P.-L. Liu, P-type conductive Ga2O3 epilayers grown on sapphire substrate by phosphorus-ion implantation technology, Mater. Today Adv. 20 (2023) 100436, https://doi.org/10.1016/j.mtadv.2023.100436.

[19] C.-Y. Huang, X.-Y. Tsai, F.-G. Tarntair, C. Langpoklakpam, T.S. Ngo, P.-J. Wang, Y.-C. Kao, Y.-K. Hsiao, N. Tumilty, H.-C. Kuo, T.-L. Wu, C.-L. Hsiao, R.-H. Horng, Heteroepitaxially grown homojunction gallium oxide PN diodes using ion implantation technologies, Mater. Today Adv. 22 (2024) 100499, https://doi.org/10.1016/j.mtadv.2024.100499.

[20] L. Li, F. Liao, X. Hu, The possibility of N–P codoping to realize P type β-Ga_2O_3, Superlattice. Microst. 141 (2020) 106502, https://doi.org/10.1016/j.spmi.2020.106502.

[21] Y. Liao, H. Song, Z. Xie, C. Zhang, C.-K. Tan, Exploration of *p*-type conductivity in *β*-Ga2O3 through Se-Mg hyper co-doped: an ion implantation approach, Mater. Today Adv. 25 (2025) 100559, https://doi.org/10.1016/j.mtadv.2025.100559.

[22] F. Alema, B. Hertog, A. Osinsky, P. Mukhopadhyay, M. Toporkov, W.V. Schoenfeld, Fast growth rate of epitaxial β–Ga2O3 by close coupled showerhead MOCVD, J. Cryst. Growth 475 (2017) 77–82, https://doi.org/10.1016/j.jcrysgro.2017.06.001.

[23] A. Hernandez, M. Minhazul Islam, P. Saddatkia, C. Codding, P. Dulal, S. Agarwal, A. Janover, S. Novak, M. Huang, T. Dang, M. Snure, F.A. Selim, MOCVD growth and characterization of conductive homoepitaxial Si-doped Ga2O3, Results Phys. (2021) 104167, https://doi.org/10.1016/j.rinp.2021.104167.

[24] G. Seryogin, F. Alema, N. Valente, H. Fu, E. Steinbrunner, A.T. Neal, S. Mou, A. Fine, A. Osinsky, MOCVD growth of high purity Ga2O3 epitaxial films using trimethylgallium precursor, Appl. Phys. Lett. 117 (2020) 262101, https://doi.org/10.1063/5.0031484.

[25] W. Li, J. Li, Y. Wang, T. Zhang, W. Wang, H. Gao, X. Tian, Y. Zhang, Q. Cheng, Q. Feng, J. Zhang, Y. Hao, Influence of oxygen on Ga2O3 deposition at low temperature by MOCVD, Cryst. Growth Des. 24 (2024) 171–178, https://doi.org/10.1021/acs.cgd.3c00815.

[26] C. Nie, K. Liu, C. Ke, X. Jiang, Y. He, Y. Deng, Y. Yan, G. Luo, Spontaneous donor defects and voltage-assisted hole doping in beta-gallium oxides under multiple epitaxy conditions, ACS Appl. Electron. Mater. 7 (2025) 788–797, https://doi.org/10.1021/acsaelm.4c01924.

[27] F. Alema, T. Itoh, W. Brand, A. Osinsky, J.S. Speck, Controllable nitrogen doping of MOCVD Ga2O3 using NH3, Appl. Phys. Lett. 122 (2023) 252105, https://doi.org/10.1063/5.0149248.

[28] Z. Feng, A.F.M. Anhar Uddin Bhuiyan, M.R. Karim, H. Zhao, MOCVD homoepitaxy of Si-doped (010) β-Ga_2O_3 thin films with superior transport properties, Appl. Phys. Lett. 114 (2019) 250601, https://doi.org/10.1063/1.5109678.

[29] D. Gogova, D.Q. Tran, V. Stanishev, V. Jokubavicius, L. Vines, M. Schubert, R. Yakimova, P.P. Paskov, V. Darakchieva, High crystalline quality homoepitaxial Si-doped β-Ga2O3(010) layers with reduced structural anisotropy grown by hot-wall MOCVD, J. Vac. Sci. Technol. A 42 (2024) 022708, https://doi.org/10.1116/6.0003424.

[30] L. Meng, D. Yu, H.-L. Huang, C. Chae, J. Hwang, H. Zhao, MOCVD growth of β-Ga2O3 on (001) Ga2O3 substrates, Cryst. Growth Des. 24 (2024) 3737–3745, https://doi.org/10.1021/acs.cgd.4c00060.

[31] C.-Y. Huang, X.-Y. Tsai, F.-G. Tarntair, A.K. Singh, S.-H. Hsu, D.-S. Wuu, K. Järrendahl, C.-L. Hsiao, R.-H. Horng, Fabrication of vertical gallium oxide PN diodes using homoepitaxial growth by MOCVD and ion implantation technology, Mater. Today Adv. 25 (2025) 100568, https://doi.org/10.1016/j.mtadv.2025.100568.

[32] G. Pozina, C.-W. Hsu, N. Abrikossova, M.A. Kaliteevski, C. Hemmingsson, Development of β-Ga2O3 layers growth on sapphire substrates employing modeling of precursors ratio in halide vapor phase epitaxy reactor, Sci. Rep. 10 (2020) 22261, https://doi.org/10.1038/s41598-020-79154-9.

[33] D. Dohy, G. Lucazeau, A. Revcolevschi, Raman spectra and valence force field of single-crystalline β Ga2O3, J. Solid State Chem. 45 (1982) 180–192, https://doi.org/10.1016/0022-4596(82)90274-2.

[34] D. Machon, P.F. McMillan, B. Xu, J. Dong, High-pressure study of the *β*-to-*α* transition in Ga_2O_3, Phys. Rev. B 73 (2006) 094125, https://doi.org/10.1103/PhysRevB.73.094125.

[35] Z. Li, T. Jiao, J. Yu, D. Hu, Y. Lv, W. Li, X. Dong, B. Zhang, Y. Zhang, Z. Feng, G. Li, G. Du, Single crystalline β-Ga2O3 homoepitaxial films grown by MOCVD, Vacuum 178 (2020) 109440, https://doi.org/10.1016/j.vacuum.2020.109440.

[36] R. Rao, A.M. Rao, B. Xu, J. Dong, S. Sharma, M.K. Sunkara, Blueshifted Raman scattering and its correlation with the [110] growth direction in gallium oxide nanowires, J. Appl. Phys. 98 (2005) 094312, https://doi.org/10.1063/1.2128044.

[37] A.G. Shard, Practical guides for x-ray photoelectron spectroscopy: quantitative XPS, J. Vac. Sci. Technol. A 38 (2020) 041201, https://doi.org/10.1116/1.5141395.

[38] K. Arora, N. Kumar, P. Vashishtha, G. Gupta, M. Kumar, Investigating the role of oxygen and related defects in the self-biased and moderate-biased performance of β-Ga2O3 solar-blind photodetectors, J. Phys. Appl. Phys. 54 (2021) 165102, https://doi.org/10.1088/1361-6463/abd9a5.

[39] S.K. Jain, P. Goel, U. Varshney, T. Garg, N. Aggarwal, S. Krishna, S. Singh, G. Gupta, Impact of thermal oxidation on the electrical transport and chemical & electronic structure of the GaN film grown on Si and sapphire substrates, Appl. Surf. Sci. Adv. 5 (2021) 100106, https://doi.org/10.1016/j.apsadv.2021.100106.

[40] T. Fan, N. Tang, J. Wei, S. Zhang, Z. Sun, G. Li, J. Jiang, L. Fu, Y. Zhang, Y. Yuan, X. Rong, W. Ge, X. Wang, B. Shen, Reduction of vacancy defects induced by thermal annealing in β-Ga2O3 epilayer, Micro Nanostruct. 176 (2023) 207525, https://doi.org/10.1016/j.micrna.2023.207525.

[41] Y. Wang, J. Li, T. Zhang, W. Wu, W. Li, Y. Yao, Z. Wang, Q. Feng, Y. Zhang, J. Zhang, Y. Hao, Enhancing the quality of homoepitaxial (−201) β-Ga2O3 thin film by MOCVD with in situ pulsed indium, Appl. Phys. Lett. 124 (2024) 072105, https://doi.org/10.1063/5.0189586.

[42] S. Bhowmick, R. Saha, M. Mishra, A. Sengupta, S. Chattopadhyay, S. Chakrabarti, Oxygen mediated defect evolution in RF sputtered Ga2O3 thin films on p-Si

substrate, Mater. Today Commun. 33 (2022) 104766, https://doi.org/10.1016/j.mtcomm.2022.104766.
[43] L.-X. Qian, Z.-H. Wu, Y.-Y. Zhang, P.T. Lai, X.-Z. Liu, Y.-R. Li, Ultrahigh-responsivity, rapid-recovery, solar-blind photodetector based on highly nonstoichiometric amorphous gallium oxide, ACS Photonics 4 (2017) 2203–2211, https://doi.org/10.1021/acsphotonics.7b00359.
[44] J. Wang, X. Ji, S. Qi, Z. Li, Z. Yan, M. Li, X. Yan, A. Zhong, C. Lu, X. Qi, P. Li, Regulation of oxygen vacancies in nitrogen-doped Ga2O3 films for high-performance MSM solar-blind UV photodetectors, J. Mater. Chem. C 11 (2023) 6202–6211, https://doi.org/10.1039/D3TC00345K.
[45] E. Chikoidze, C. Sartel, H. Mohamed, I. Madaci, T. Tchelidze, M. Modreanu, P. Vales-Castro, C. Rubio, C. Arnold, V. Sallet, Y. Dumont, A. Perez-Tomas, Enhancing the intrinsic p-type conductivity of the ultra-wide bandgap Ga_2O_3 semiconductor, J. Mater. Chem. C 7 (2019) 10231–10239, https://doi.org/10.1039/c9tc02910a.
[46] M.E. Ingebrigtsen, A.Yu Kuznetsov, B.G. Svensson, G. Alfieri, A. Mihaila, U. Badstübner, A. Perron, L. Vines, J.B. Varley, Impact of proton irradiation on conductivity and deep level defects in β-Ga $_2$ O $_3$, APL Mater. 7 (2019) 022510, https://doi.org/10.1063/1.5054826.
[47] E. Chikoidze, A. Fellous, A. Perez-Tomas, G. Sauthier, T. Tchelidze, C. Ton-That, T. T. Huynh, M. Phillips, S. Russell, M. Jennings, B. Berini, F. Jomard, Y. Dumont, P-type β-gallium oxide: a new perspective for power and optoelectronic devices, Mater. Today Phys. 3 (2017) 118–126, https://doi.org/10.1016/j.mtphys.2017.10.002.
[48] E. Serquen, F. Bravo, Z. Chi, L.A. Enrique, K. Lizárraga, C. Sartel, E. Chikoidze, J. A. Guerra, Impact of c- and m- sapphire plane orientations on the structural and electrical properties of β-Ga2O3 thin films grown by metal-organic chemical vapor deposition, J. Phys. Appl. Phys. 57 (2024) 495106, https://doi.org/10.1088/1361-6463/ad76bb.
[49] S. Cho, J. Lee, I.-Y. Park, S. Kim, New luminescence band due to nitrogen impurities in gallium oxide powders, Mater. Lett. 57 (2002) 1004–1009, https://doi.org/10.1016/S0167-577X(02)00914-X.
[50] A. Luchechko, V. Vasyltsiv, M. Kushlyk, D. Slobodzyan, M. Baláž, J. Cebulski, K. Szmuc, J. Szlęzak, Y. Shpotyuk, Structural and luminescence characterization of β-Ga2O3 nanopowders obtained via high-energy ball milling, Appl. Nanosci. 13 (2023) 5149–5155, https://doi.org/10.1007/s13204-022-02717-x.
[51] Y. Nie, S. Jiao, S. Li, H. Lu, S. Liu, S. Yang, D. Wang, S. Gao, J. Wang, Y. Li, Modulating the blue and green luminescence in the β-Ga2O3 films, J. Alloys Compd. 900 (2022) 163431, https://doi.org/10.1016/j.jallcom.2021.163431.
[52] T. Onuma, S. Fujioka, T. Yamaguchi, M. Higashiwaki, K. Sasaki, T. Masui, T. Honda, Correlation between blue luminescence intensity and resistivity in β-Ga2O3 single crystals, Appl. Phys. Lett. 103 (2013) 041910, https://doi.org/10.1063/1.4816759.
[53] L.T. Penman, Z.M. Johnston, P.R. Edwards, Y. Oshima, C. McAleese, P. Mazzolini, M. Bosi, L. Seravalli, R. Fornari, R.W. Martin, F.C.-P. Massabuau, Comparative study of the optical properties of α-, β-, and κ-Ga2O3, Phys. Status Solidi B n/a (2025) 2400615, https://doi.org/10.1002/pssb.202400615.
[54] M. Meißner, N. Bernhardt, F. Nippert, B.M. Janzen, Z. Galazka, M.R. Wagner, Anisotropy of optical transitions in β-Ga2O3 investigated by polarized photoluminescence excitation spectroscopy, Appl. Phys. Lett. 124 (2024) 152102, https://doi.org/10.1063/5.0189751.
[55] L. Binet, D. Gourier, ORIGIN OF THE BLUE LUMINESCENCE OF β-Ga2O3, J. Phys. Chem. Solid. 59 (1998) 1241–1249, https://doi.org/10.1016/S0022-3697(98)00047-X.
[56] Q.D. Ho, T. Frauenheim, P. Deák, Origin of photoluminescence in β-Ga_2O_3, Phys. Rev. B 97 (2018) 115163, https://doi.org/10.1103/PhysRevB.97.115163.